Direct observation of LO phonon-plasmon coupled modes in the infrared transmission spectra of n-GaAs and n-InxGa1-xAs epilayers

J. Ibanez* E. Tarhan† A. K. Ramdas‡
S. Hernandez** R. Cusco†† L. Artus‡‡
M. R. Melloch§ M. Hopkinson¶

*
†
‡
**
††
‡‡
§
¶

Direct observation of LO phonon-plasmon coupled modes in the infrared transmission spectra of *n*-GaAs and *n*-$In_xGa_{1-x}As$ epilayers

J. Ibáñez,* Enver Tarhan, and A. K. Ramdas
Department of Physics, Purdue University, West Lafayette, Indiana 47907-1396, USA

S. Hernández, R. Cuscó, and L. Artús
Institut Jaume Almera, Consell Superior d'Investigácions Científiques (CSIC), Lluís Solé i Sabarís s.n., 08028 Barcelona, Spain

M. R. Melloch
School of Electrical Engineering, Purdue University, West Lafayette, Indiana 47907-1390, USA

M. Hopkinson
Department of Electronics and Electrical Engineering, University of Sheffield, Sheffield S1 3JD, United Kingdom
(Received 20 March 2003; revised manuscript received 30 October 2003; published 26 February 2004)

The infrared transmission spectrum of Si-doped molecular beam epitaxy (MBE)-grown GaAs epilayers, 2–2.5-μm thick, measured in the oblique (Berreman) geometry, revealed distinct minima in *p* polarization. Given epilayer thickness $\ll$ *reststrahlen* wavelength, the minima are identified as the zone-center transverse optic phonon (ω_{TO}) and the high-frequency LO phonon-plasmon coupled mode (ω_+). Analysis of the experimental data yielded free-carrier concentrations ranging from 2.5×10^{17} to 1.4×10^{18} cm^{-3}. The same technique with MBE-grown Si-doped $In_{0.53}Ga_{0.47}As$ epilayers (0.5–1 μm thick) yielded ω_+ modes corresponding to free-carrier concentrations of 8.2×10^{16}–2.7×10^{19} cm^{-3}. The observations of the transmission minima in the Berreman geometry and their interpretation demonstrate a direct and simple method for deducing free-carrier concentrations over a wide range.

DOI: 10.1103/PhysRevB.69.075314 PACS number(s): 78.30.Fs

I. INTRODUCTION

The plasma edge associated with free carriers in semiconductors was first observed and delineated by Spitzer and Fan.[1] In the partially ionic compound semiconductors, the plasma frequency can be tuned to the vicinity of reststrahlen by controlling the free-carrier concentration. Under these conditions, coupled plasmon-LO (longitudinal optic) phonon modes (L^+ and L^- with frequencies ω_+ and ω_-, respectively) were predicted by Yokota[2] and Varga[3]; in a quantum-mechanical formulation, Singwi and Tosi,[4] deduced phonon strengths, sum rules, and the explicit structure of the coupling term.

These coupled modes can be directly observed in the Raman spectrum of a zinc-blende polar semiconductor with free carriers as strikingly demonstrated by Mooradian and co-workers in their seminal Raman spectroscopic study of *n*-GaAs.[5,6] The phenomenon of coupled plasmon-phonon modes in Raman scattering has attracted many investigations in the context of the novel, underlying microscopic aspects in different binary semiconductors.[7,8] Raman study of the plasmon-phonon coupled modes in ternary alloys of III-Vs, by Yuasa *et al.*[9] for *n*-$Al_xGa_{1-x}As$ and by Cuscó *et al.*[10] for *n*-$In_{0.53}Ga_{0.47}As$, emphasized the occurrence of coupling between plasmons and both AlAs-like and GaAs-like LO modes in the former and InAs-like and GaAs-like LO modes in the latter; in addition, the appearance of a new coupled mode L_0 intermediate between L^+ and L^- was reported. It should be noted that the coupled modes are characterized by LO-phonon-like polarizability tensors and, consequently, allowed for backscattering from a (100) face but forbidden when from $(1\bar{1}0)$ in Raman spectroscopy.

The ω_+ and ω_- frequencies can also be deduced from an infrared reflectivity study of polar semiconductors with a significant free-carrier contribution as shown, for instance, in Chandrasekhar and Ramdas[11] for *n* GaAs. The procedure involved the calculation of the zeros of the dielectric function, i.e., ω_+ and ω_-, from a curve fitting of the reflectivity spectrum using damping constants, ω_{TO} and ω_{LO} (the zone-center optical phonon frequencies), and the effective mass of the free carriers as adjustable parameters, on the one hand, and the carrier concentrations from the measured Hall coefficient, as an input, on the other hand. We also note that Holm *et al.*[12] have studied the IR reflectivity of *n*-type GaAs samples with a focus on the determination of free-carrier concentrations. Kim and Spitzer,[13] in their infrared reflectivity study of bulk Te-doped $Al_xGa_{1-x}As$ ternary, $0\leqslant x \leqslant 0.47$, discovered the appearance of the third coupled plasmon-phonon mode, labeled L_0 in Ref. 9.

In the context of the above discussion, the Berreman effect[14,15] viz. the manifestation of the transmission minima of a very thin film of a doped semiconductor at ω_{TO}, ω_+, and ω_-, examined in oblique geometry, provides an experimental determination of their frequencies as direct as in Raman scattering. The only requirement is that the sample thickness should be significantly smaller than the reststrahlen wavelength.[14,15] Here we also refer to Grosse *et al.*[16] for an early report of the Berreman effect in reflection, another Berreman geometry in which a weak dip at ω_{TO}, and stronger ones at ω_+ and ω_- are observed. Up to date, no experimental observation of LO phonon-plasmon coupled modes in infrared transmission measurements has been reported.

In the present paper, we report the direct observation of LO phonon-plasmon coupled modes in the oblique-incidence-infrared-transmission spectra of thin, doped semiconductor epilayers by taking advantage of the Berreman effect. The experiments were carried out on a series of Si-doped GaAs and InGaAs epilayers with a wide range of free-carrier concentrations. The ω_{TO} and ω_{+} frequencies are observed as transmission minima and the free-carrier concentrations as well as damping constants are deduced from their analysis.

II. EXPERIMENT

We carried out infrared transmission experiments on a series of *n*-type GaAs and $In_{0.53}Ga_{0.47}As$ layers. GaAs layers with nominal free-carrier concentrations between 3×10^{17} and $10^{18}\,\mathrm{cm}^{-3}$ were grown by molecular beam epitaxy (MBE) on GaAs substrates after inserting a 200-Å AlAs spacer layer. The GaAs layers were separated from the substrate by the selective etching of the AlAs layers and subsequently floating them onto a Si wafer. A series of Si-doped $In_{0.53}Ga_{0.47}As$ layers with carrier concentrations in the 5×10^{16}–$5\times10^{19}\,\mathrm{cm}^{-3}$ range were grown by MBE either on n^{+} or semi-insulating (Fe doped) InP substrates. To avoid absorption by the free carriers in the substrate, the n^{+} InP buffers were selectively etched and the remaining $In_{0.53}Ga_{0.47}As$ layers were floated onto Si wafers. Nominally undoped control samples for both GaAs and $In_{0.53}Ga_{0.47}As$ layers were also prepared.

The free-electron density of the $In_{0.53}Ga_{0.47}As$ samples grown on semi-insulating InP substrates was determined from Hall measurements in the van der Pauw geometry, assuming the Hall factor as unity and using the measured epilayer thickness of 470 nm. For the $In_{0.53}Ga_{0.47}As$ samples grown on n^{+} InP substrates, the carrier concentration was determined by means of capacitance-voltage (CV) measurements using a Bio-Rad electrochemical CV profiler.

Unpolarized infrared transmission spectra were obtained in the normal and oblique geometry using a BOMEM DA3 rapid scanning Fourier-transform spectrometer. In this spectrometer, the angle of the beam splitter with respect to the optical axis is selected by the manufacturer to be 30° in order to minimize the partial polarization of the unpolarized incident light produced by the reflections at the beam splitter. For measurements from 150 to 700 cm^{-1}, a globar source, a mylar beam splitter of appropriate thickness, and a composite Si bolometer operating at 4.2 K with a long-pass cold filter and cone optics were used. In the spectral range from 700 to 5000 cm^{-1}, a globar source, a KBr beam splitter, and an MCT (HgCdTe) detector were employed. Spectra were typically recorded with 0.5 cm^{-1} resolution and 100 coadditions. All measurements were performed at 5 K using a Janis 10DT Supervaritemp optical cryostat with polypropylene windows for the far-infrared spectral range and ZnS (inner) and CsI (outer) windows in the mid infrared. By rotating the sample rod, the angle θ_i between the incident beam and the normal to the sample surface could be set. All of the Si wafers and the semi-insulating InP substrates that were not etched in the $In_{0.53}Ga_{0.47}As$ samples were polished and a wedge was deliberately introduced to avoid channeling in the spectra.

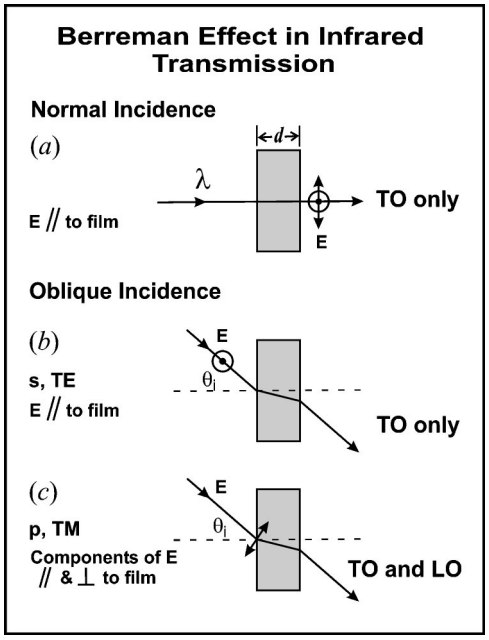

FIG. 1. Berreman effect in infrared transmission through a thin film ($d \ll \lambda$). (a) Normal incidence, only TO minimum is observed. (b) Oblique incidence, *s* (TE) polarization: only TO is observed. (c) Oblique incidence, *p* (TM) polarization: both TO and LO are observed.

III. THEORETICAL CONSIDERATIONS

On the basis of an insightful physical argument as well as simple theoretical considerations, Berreman[14] demonstrated that the transmission spectrum of a free standing polar crystal should exhibit a minimum at transverse optic (TO) zone center optical frequencies at *normal incidence*, while at *oblique incidence*, minima are observed at both TO and LO frequencies. In addition, the TO modes are observed for both *s* and *p* polarizations whereas LO appears only in the *p* polarization. Proix and Balkanski[17] summarized the theoretical analysis of Kliewer and Fuchs[18] who considered the transmission and reflectivity of an ionic slab and concluded that, for thickness *d* satisfying $(\omega_{\mathrm{TO}}d/c \ll 1)$, the positions of the transmission minima indeed correspond to those of the bulk ω_{TO} and ω_{LO} as deduced by Berreman.

Consider $\omega_{\mathrm{TO}}d/c \ll 1$ to be satisfied by a zinc-blende polar semiconductor film (i.e., equivalently, $\lambda_{\mathrm{TO}} \gg d$). For such a film one can visualize two uniform normal modes of vibration. The equation of motion of the positive and negative ions, together with a depolarizing electric field of $-4\pi\mathbf{P}$ where $\mathbf{P}$ is normal to the plane and zero when in the plane, indeed yield the ω_{TO} and ω_{LO} frequencies which fulfill the well-known Lydanne-Sachs-Teller relation. The appearance of ω_{TO} minimum in the *s* and *p* polarization for both normal and oblique transmission in contrast to that of ω_{LO} in only oblique transmission and *p* polarization follows naturally (Fig. 1). In Sciacca *et al.*,[15] the success of the Berreman technique is immediately apparent in Table II as well as in the

polarization characteristics verified for a large number of polar crystals as well as superlattices.

As is well known,[2,3] the dielectric function for a zinc-blende polar semiconductor, including the contribution of free carriers is given by

$$\epsilon(\omega)=\epsilon_\infty+\frac{\epsilon_0-\epsilon_\infty}{1-(\omega/\omega_{\mathrm{TO}})^2-i\gamma(\omega/\omega_{\mathrm{TO}})}$$

$$-\frac{\epsilon_\infty}{(\omega/\omega_p)^2+i\gamma_p(\omega/\omega_p)}, \tag{1}$$

where γ (γ_p) is the phonon (plasmon) damping coefficient, $\omega_p=[4\pi N_e e^2/(m^*\epsilon_\infty)]^{1/2}$ is the plasma frequency, N_e is the free-carrier concentration, and m^* is the free-carrier effective mass. The damping constants specified in the context of experimental results are conveniently expressed in units of cm^{-1}; therefore we use $\Gamma_{\mathrm{ion}}=\gamma\omega_{\mathrm{TO}}$ and $\Gamma_e=\gamma_p\omega_p$.

For a two-mode ternary alloy $A_xB_{1-x}C$ such as $\mathrm{In}_x\mathrm{Ga}_{1-x}\mathrm{As}$, the ionic lattice contribution to the dielectric function can be expressed in terms of the contributions from the two polar sublattices[19]

$$\epsilon_{\mathrm{ion},x}(\omega)=\sum_{i=A,B}x_i\epsilon_{\infty,i}\frac{(\omega^0_{\mathrm{LO},i})^2-(\omega^0_{\mathrm{TO},i})^2}{\omega^2_{\mathrm{TO},i}-\omega^2-i\Gamma_i\omega}, \tag{2}$$

where $i=A,B$ indicates the alloy sublattice, Γ_i is the damping constant for the phonons of the i sublattice, $\omega^0_{\mathrm{LO},i}$ and $\omega^0_{\mathrm{TO},i}$ are the LO and TO phonon frequencies of the pure end-member compounds and $\omega_{\mathrm{TO},i}$ is the TO phonon frequency of the i alloy sublattice. Within this formalism, the high-frequency dielectric constant for the alloy is given by the weighted average between the values of the pure end-member compounds

$$\epsilon_\infty(x)=\sum_{i=A,B}x_i\epsilon_{\infty,i}. \tag{3}$$

The dielectric function of a two-mode ternary alloy including the contribution of free carriers is then obtained from the expression for a binary zinc-blende semiconductor [Eq. (1)] by replacing the ionic lattice contribution [second term of Eq. (1)] by Eq. (2), and ϵ_∞ by Eq. (3).

The effective mass has been calculated as a function of Fermi level including the conduction-band nonparabolicity.[11,20] This is achieved by using the optical effective mass, which, for an isotropic band, is given by[21]

$$\frac{1}{m^*_{\mathrm{op}}}=\frac{1}{3\pi^2\hbar^2N_e}\int_0^{k_F(E_F)}\frac{\partial}{\partial k}\left(k^2\frac{\partial E(k)}{\partial k}\right)dk, \tag{4}$$

where k_F is the wave vector at the Fermi energy E_F. The conduction-band dispersion was obtained for GaAs and $\mathrm{In}_{0.53}\mathrm{Ga}_{0.47}\mathrm{As}$ from a 14×14 $\mathbf{k}\cdot\mathbf{p}$ calculation that included the interactions among the Γ_7 split-off valence bands, the Γ_8 valence bands, and the Γ_6, Γ_7, and Γ_8 conduction bands.[22] The critical point energies and the matrix elements for the $\mathbf{k}\cdot\mathbf{p}$ calculation are those of Ref. 23. For $\mathrm{In}_{0.53}\mathrm{Ga}_{0.47}\mathrm{As}$, composition-weighted averages of the corresponding values of InAs and GaAs were used in the spirit of virtual crystal approximation. An isotropic energy dispersion was derived by averaging over a suitable set of high-symmetry directions in k space, and a polynomial expansion $E(k)=A_2k^2+A_4k^4+A_6k^6$ was fitted to the $\mathbf{k}\cdot\mathbf{p}$ results.[24] The relationships between Fermi energy and electron density, and between Fermi wave vector and Fermi energy, required for evaluating Eqs. (1) and (4), are also determined by expansions up to terms in k^6.

The zeros of the dielectric function yield the frequencies of the coupled LO phonon-plasmon modes.[25] The dielectric function $\epsilon=\epsilon_1+i\epsilon_2$ is related to the real and imaginary parts of the complex refractive index, $\tilde{n}=n+i\kappa$ (κ: extinction coefficient) by

$$n^2-\kappa^2=\epsilon_1,$$

$$2n\kappa=\epsilon_2. \tag{5}$$

The fractional transmission of a thin film of thickness d and complex dielectric function $\epsilon(\omega)=\tilde{n}^2(\omega)$ for TE (s-polarized) electromagnetic radiation of frequency ω incident on the film at an angle θ_i is[15]

$$T_{\mathrm{TE}}=\left|\left[\cos\kappa d-i\left(\frac{\kappa^2+k^2}{2\kappa k}\right)\sin\kappa d\right]^{-1}\right|^2, \tag{6}$$

while for TM (p-polarized) waves[15]

$$T_{\mathrm{TM}}=\left|\left[\cos\kappa d-i\left(\frac{\kappa^2+n^4k^2}{2n^2\kappa k}\right)\sin\kappa d\right]^{-1}\right|^2. \tag{7}$$

Here, $k=(\omega/c)\cos\theta_i$ and $\kappa=(\omega/c)[n^2-\sin^2\theta_i]^{1/2}$. When the incident light is unpolarized, the total transmission of the film is obtained by averaging over all the polarization directions, and the fractional transmission becomes

$$T=\tfrac{1}{2}(T_{\mathrm{TE}}+T_{\mathrm{TM}}). \tag{8}$$

(N_e/m^*_{op}) is calculated as a function of E_F in terms of A_2, A_4, and A_6 (see values in Ref. 24) and inserted into the expression for ω_p and, in turn, into Eq. (1). Treating N_e, and Γ_e as adjustable parameters, they are deduced by a curve-fitting procedure applied to the spectrum of the fractional transmission [Eq. (8)].

IV. COUPLED MODES: INFRARED VS RAMAN SCATTERING

It should be noted that the infrared and Raman experiments involve wave vectors q with very different magnitudes, and this has a bearing on the behavior of the coupled modes observed in the two techniques. While in infrared experiments one can assume that the plasma excitations have zero wave vector, the wave vector of the plasmons involved in Raman experiments with visible excitation is not negligible. The spatial distribution of the polarization field associated with the coupled modes excited in Raman experiments is different from that of the coupled modes excited in infra-

red measurements, and this is reflected in the coupled mode behavior as discussed below.

In *n*-type binary polar semiconductors such as *n*-GaAs, the coupling of the LO phonon mode with the free carriers gives rise to two coupled modes, labeled L^- and L^+ corresponding to their frequencies, ω_- and ω_+, respectively.[8] In the low-damping regime, the frequency of these modes are given by the zeros of the dielectric function. In the small-q limit, the L^- mode displays plasmon-like character when ω_p is much smaller than ω_{LO}, and becomes phonon-like, with a frequency that approaches ω_{TO}, when the plasma frequency is much greater than the LO frequency. Conversely, the L^+ mode is phonon-like in character with a frequency that approaches ω_{LO} when $\omega_p \ll \omega_{\mathrm{LO}}$, and becomes a plasmon-like mode when $\omega_p \gg \omega_{\mathrm{LO}}$.

The half-widths of the L^+ and L^- signatures also correspondingly exhibit the admixture of those of the plasmon and LO phonon. Following Varga,[3] one can specify the relative contributions to the coupled mode from the LO phonon and the plasmon. Mooradian and Wright[5] have given an analytical expression for the admixture in Eq. (3) and illustrated in Fig. 3 of Ref. 5. For low N_e, the phonon contribution dominates that of the plasmon for L^+ and vice versa for L^-, whereas the reverse situation prevails at high N_e's. In the same spirit, the half-width of L^+ will be governed by that of the LO phonon at small N_e and by that of the plasmon at large N_e; for L^- the situation is reversed.

The nature of the coupled plasmon-phonon modes in multinary alloys is altered significantly as a consequence of the multimode behavior of their zone-center optical modes.[9,10,13] In a ternary semiconductor with two-mode behavior, the LO modes of both sublattices couple with the free-carrier excitations. Then, in the low-damping regime and in the small-q limit, which is relevant for the infrared measurements, the corresponding dielectric function exhibits three zeros that are associated with the L^-, L_0, and L^+ coupled modes. Consider $In_{1-x}Ga_xAs$, the case of interest in the present paper; it has InAs-like LO-TO and GaAs-like LO-TO pairs, the members of the former at lower frequencies than their counterparts of the latter. In the low-damping regime and small-q limit, the coupled mode behavior is as follows: (1) As a function of N_e, L^+ starts out as GaAs-like LO and becomes plasmon-like beyond the crossover of ω_{LO} and ω_p; (2) L^-, plasmon-like for small N_e, asymptotically transforms to InAs-like TO for large N_e. (3) The feature, L_0, predominantly InAs-like LO for small N_e becomes essentially GaAs-like TO at large N_e's. L^+ and L^- exhibit complementary phonon-like and plasmon-like behavior while L_0 begins with a large InAs-like LO phonon-like fraction, for small N_e and asymptotically GaAs-like TO at large N_e, but plasmon-like for $\omega_{\mathrm{LO}}(\mathrm{InAs}) < \omega_p < \omega_{\mathrm{TO}}(\mathrm{GaAs})$. Such behavior is exemplified in Figs. 8 and 9 of Yuasa *et al.*,[9] where the evolution of L^+, L_0, and L^-, and the plasmon content in each of them are displayed as a function of N_e, respectively, in the analogous case of $Al_{1-x}Ga_xAs$. (Note that GaAs-like TO-LO is the low-frequency pair in $Al_{1-x}Ga_xAs$ whereas it is the high-frequency pair in $In_{1-x}Ga_xAs$). The coupled mode behavior depicted above can be derived from a Drude model of the free-carrier contribution to the electric susceptibility. This model gives a good description of the coupled modes away from the Landau damping region. Landau damping becomes negligible for $q \to 0$ and therefore the use of this model in Sec. III for the analysis of the infrared transmission measurements is justified.

However, one has to recognize that the coupled mode behavior as described above can be substantially altered in the Landau damping region where plasmons decay into single-particle excitations. In Raman-scattering measurements with visible excitation, the magnitude of the wave vectors involved in the scattering process makes the Landau damping region extend to the spectral region where coupled modes occur, particularly, in compounds with small electron effective mass and low optical phonon frequencies. In the Raman-scattering investigation of the same *n*-$In_{0.53}Ga_{0.47}As$ epilayers by Cuscó *et al.*,[10] the significance of Landau damping became evident in view of the low effective mass of the free carriers. A more elaborate model based on the Lindhard-Mermin susceptibility is then appropriate for the analysis of the Raman experiments. In this case, instead of the L_0 and L^- coupled modes, two heavily damped coupled modes occur at frequencies that decrease with increasing carrier density and asymptotically approach the TO mode frequencies of the alloy. Given the small wave vector of the far-infrared light, decay of the coupled modes into single-particle excitations is not relevant in infrared measurements, and an analysis based on Eqs. (1) and (4) is adequate in the interpretation of our infrared transmission results.

V. RESULTS AND DISCUSSION

A. Coupled modes in GaAs

The infrared transmission spectra at 5 K obtained at oblique incidence ($\theta_i \approx 45°$) for the four GaAs epilayers investigated are displayed in Fig. 2(a). Sample *A* is nominally undoped, whereas the nominal doping concentration for samples *B*, *C*, and *D* is 3×10^{17}, 6×10^{17}, and 10^{18} cm^{-3}, respectively. For clarity, the spectra have been shifted vertically in the figure.

The GaAs TO mode is observed in the spectrum of the undoped sample (*A*) as a broad transmission minimum centered at 271.6 cm^{-1}. In addition, the narrow dip located at 293.4 cm^{-1}, observed in the transmission spectra at oblique incidence, can be unambiguously assigned to the LO phonon mode which interacts with the radiation polarized parallel to the plane of incidence giving rise to the Berreman effect.[14,15]

The transmission spectra of the *n*-type GaAs epilayers (*B*–*D*) at oblique incidence exhibit three main features. First, the minimum associated with TO phonon absorption is asymmetrically broadened towards higher wave numbers due to free-carrier absorption. Second, just below the TO frequency, a dip located at about 263 cm^{-1} can be seen in all spectra. Absorption by LO phonon-plasmon coupled modes, i.e., by the L^- mode, can be ruled out as the origin of this dip since, as can be seen in the inset of Fig. 2(a), it also appears in the spectra at normal incidence. Dips below the TO frequency have been identified as interference fringes resulting from the rapid increase of the dielectric function below the

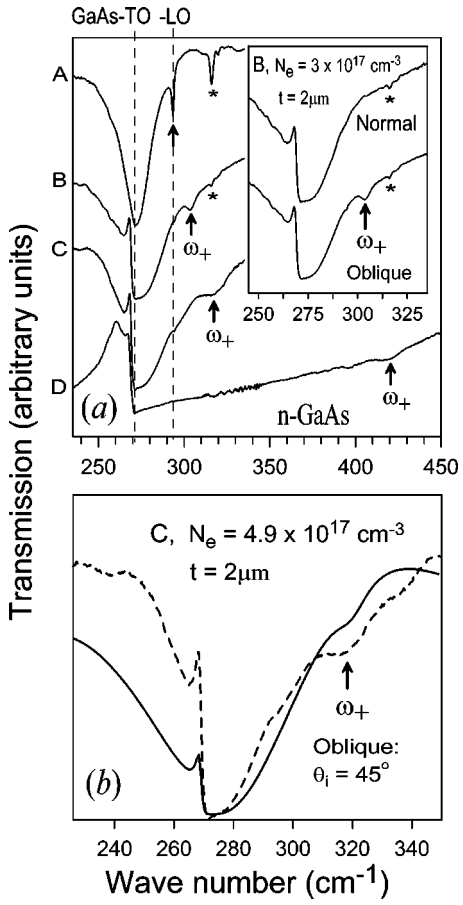

FIG. 2. (a) Infrared transmission spectra at oblique incidence of GaAs samples with different nominal doping levels: *A*, undoped; *B*, 3×10^{17} cm^{-3}; *C*, 6×10^{17} cm^{-3}; *D*, 10^{18} cm^{-3}. The arrows indicate the transmission dips due to the L^+ coupled modes. Inset, comparison between the infrared transmission of sample *B* obtained at normal and oblique incidence. The transmission dip indicated by (*) is due to the $1s(A_1)\rightarrow 2p_\pm$ transition of electrons bound to residual P donors in the Si substrate.[26] (b) Infrared transmission calculated for oblique incidence ($\theta_i=45°$), $N_e=4.9\times10^{17}$ cm^{-3} and $\Gamma_e=50$ cm^{-1} (solid line) compared with the experimental spectrum of sample *C* (dotted line).

pole at ω_{TO}.[15] We will further discuss this point below. The third feature is a transmission dip, indicated by the arrows in Fig. 2 that shifts to higher wave numbers with increasing free electron concentration. These transmission minima, located at 304, 316, and 418 cm^{-1} in spectra *B*, *C*, and *D*, respectively, do not appear at normal incidence, as can be seen in the inset to Fig. 2, for sample, *B*. Given their dependence on the electron density and their appearance only in oblique incidence, they can be assigned to infrared absorption by L^+ modes. This assignment is further supported by the calculations carried out using the theoretical model outlined in Sec. III. The values of ω_{TO} (271.6 cm^{-1}) and ω_{LO} (293.4 cm^{-1}) given above and $\epsilon_\infty=10.9$ (Ref. 23) together with $\Gamma_{\mathrm{ion}}=1.2$ cm^{-1} ($\Gamma_{\mathrm{ion}}=\gamma\omega_{\mathrm{TO}}$) yield a good fit to the observed width of the transmission minima in the undoped sample. Thus, we used these values to calculate the transmission curves of the doped samples on both normal and oblique incidence. As an illustrative example, we compare in Fig. 2(b) the experimental and calculated infrared transmission curves for sample *C*. The solid line is the calculated transmission spectrum at $\theta_i=45°$ for $N_e=4.9\times10^{17}$ cm^{-3}, $\Gamma_e=45$ cm^{-1} ($\Gamma_e=\gamma_p\omega_p$), and a nominal thickness of 2 μm. It is important to note that the dips assigned to the L^+ mode are present in transmission curves calculated for oblique incidence only. In contrast, the transmission dip occurring at a frequency slightly lower than the TO frequency appears in the curves calculated at normal as well as oblique incidence, indicating that it is not related to L^-.

We have not been able to identify a spectral feature at the position of L^- deduced from that of L^+. This is not surprising in view of the earlier discussion on the relative damping constants of the LO phonon and the plasmon. For small N_e, L^- is weak and plasmon-like, hence broad while for large N_e, it merges with the strong TO minimum. In contrast, for small N_e, L^+ occurs close to the LO phonon position but on its own; it can thus be unambiguously identified, having an LO-phonon-like damping constant due to the larger phonon content. For larger N_e, the absorption by the L^+ mode becomes stronger, and though broad because of the larger plasmon content, the L^+ mode is still discernible.

The transmission data can be used to determine the free-carrier concentration N_e in the doped layers by fitting the calculated line shape to the experimental curves with N_e and the electronic damping Γ_e as free parameters. To this end, we have adjusted the values of N_e and Γ_e to yield the calculated curves for the L^+ minima most consistent with the experimental spectra. Whereas the frequency of the L^+ is quite sensitive to N_e, and therefore permits an accurate determination of the carrier density, it shows negligible dependence on the electronic damping parameter Γ_e. The magnitude and shape of the L^+ transmission minima are very sensitive to the angle of incidence, hence the latter has to be set very precisely for accurate determination of Γ_e.

The carrier concentrations obtained from the theoretical fit to the transmission spectra of the GaAs epilayers are listed in Table I; it can be seen that the carrier concentrations thus obtained are close to the nominal doping levels of the layers. Therefore, we conclude that the measurement of the L^+ frequency observed in the Berreman geometry provides an alternative optical technique for a reliable determination of the free-carrier density in doped semiconductor layers. Due to the inherent large width of L^+ and the uncertainty associated with the angle of incidence, the trend in the values of Γ_e can be established only qualitatively; within this limitation, it appears to increase with N_e as seen in Table I.

B. Coupled modes in $In_{0.53}Ga_{0.47}As$

We have also investigated L^+, L_0, and L^- modes manifested by the *n*-type ternary alloy $In_{0.53}Ga_{0.47}As$ in the infrared as a result of the Berreman effect. Because of the small electron effective mass in $In_{0.53}Ga_{0.47}As$, the frequencies of the L^+ modes in this compound are particularly sensitive to the free electron concentration. Thus, L^+ frequencies range from 280 cm^{-1} to 1530 cm^{-1} as N_e increases from 10^{17} to 3×10^{19} cm^{-3}.[10] In Fig. 3(a), we display the infrared trans-

TABLE I. List of the GaAs epilayers studied in this work. d is the nominal thickness of the epilayers. The third column lists the observed ω_+ frequencies. The values of free-carrier density N_e listed in the fourth column are the nominal doping concentrations. The free-electron concentrations and damping parameters obtained from fitting the theoretical curves to the experimental transmission spectra at oblique incidence have been listed in the fifth and sixth columns, respectively.

Sample	d (μm)	$\omega+$ (cm$-$1)	N_e (cm^{-3})	N_e^{IR} (cm^{-3})	Γe (cm^{-1})
A	2		undoped		
B	2	304	3×10^{17}	2.6×10^{17}	40
C	2	316	6×10^{17}	4.9×10^{17}	45
D	2.5	418	1×10^{18}	1.4×10^{18}	50

mission spectra at 5 K in oblique incidence for n-$In_{0.53}Ga_{0.47}As$ layers for low free-carrier concentrations, *viz.* 1.1×10^{17} and 1.8×10^{17} cm^{-3}, as determined by CV measurements. The spectrum of an undoped $In_{0.53}Ga_{0.47}As$ sample (E) is also shown for reference.

The InAs-like and GaAs-like TO phonon modes (characteristic of ternaries with two-mode zone-center optical phonons) are clearly observed in the spectra as pronounced transmission minima at 228.3 and 258.4 cm^{-1}, respectively. These frequencies are in good agreement with the Raman values in the literature.[27] A shoulder can be clearly seen at $\sim$247 cm^{-1} in the spectrum of the undoped layer (E); it corresponds to a feature associated with disorder in the ternary previously reported in its Raman spectrum.[27] Further, a clear transmission dip appears at 273.2 cm^{-1} in the spectrum E, corresponding to the GaAs-like LO mode, consistent with Raman scattering results.[10,27] No dip is observed at the InAs-like LO mode frequency, probably due to the small LO-TO splitting of the InAs-like modes, in turn resulting in the overlap of the InAs-like LO dip with the stronger broad transmission minimum associated with the InAs-like TO mode.

We have applied the theoretical model of Sec. III to calculate transmission curves at oblique incidence for the n-$In_{0.53}Ga_{0.47}As$ samples. The two-mode nature of $In_{1-x}Ga_xAs$ is suitably taken into account by using Eq. (2) for the calculation of the ionic contribution to the dielectic function. The TO frequencies entering Eq. (2) were taken from Table II of Ref. 10, and a value of $\epsilon_\infty=11.5$ was obtained as the weighted average of the corresponding values for the end members.

Figure 3(b) shows the calculated transmission at $\theta_i=45°$ for $N_e=1.6\times10^{17}$ cm^{-3} and $\Gamma_e=20$ cm^{-1}. The theoretical curve (solid line) shows transmission dips at the InAs-like and GaAs-like TO frequencies that closely resemble those observed in the experimental spectrum (dotted line). As can be seen in Fig. 3(b), the oblique incidence calculations also yield transmission minima at the L^+ mode frequency that are in excellent agreement with the dips observed in the experimental spectra.

For the doped samples, a transmission dip appears whose position shifts to higher frequencies with increasing free-carrier concentration. As seen in Fig. 3(a), ω_+ for sample F occurs at 278 cm^{-1} as compared with 285 cm^{-1} for G consistent with their nominal concentrations of 5×10^{16} and 1×10^{17} cm^{-3}, respectively. As shown in the inset of Fig. 3(a) for sample F, these dips labeled ω_+ do not appear in normal incidence, and hence they can be assigned to coupled LO phonon-plasmon modes. This behavior clearly identifies them as the L^+ coupled modes.

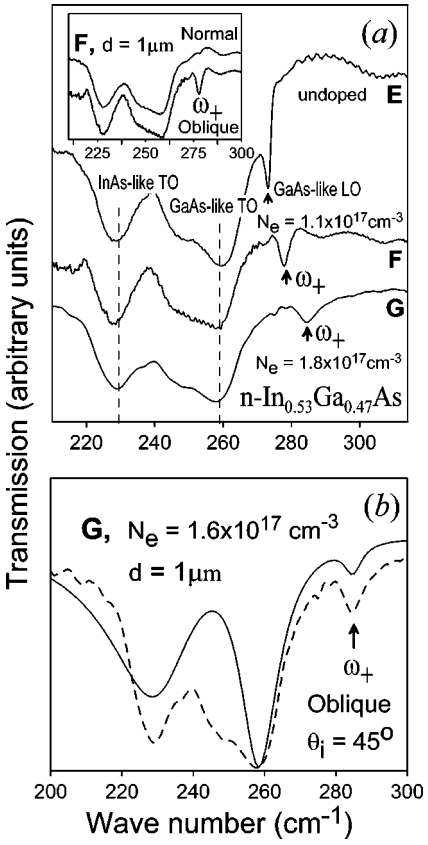

FIG. 3. (a) Infrared transmission spectra at oblique incidence of n-$In_{0.53}Ga_{0.47}As$ samples with different electron concentrations: E, undoped; F, 1.1×10^{17} cm^{-3}; G, 1.8×10^{17} cm^{-3}. Inset, comparison between the infrared transmission of sample F obtained at normal and oblique incidence. (b) Infrared transmission calculation carried out for oblique incidence ($\theta_i=45°$) for $N_e=1.6\times10^{17}$ cm^{-3} and $\Gamma_e=20$ cm^{-1} (solid line) compared with the experimental spectrum of sample G (dotted line).

Due to free-carrier absorption, the more heavily doped n-$In_{0.53}Ga_{0.47}As$ samples (H-K) exhibit a very low transmission in the optical phonon region. However, as can be seen in Fig. 4(a), a clear transmission dip can still be observed at higher frequencies in these samples. The frequency of this dip markedly increases with increasing electron concentration and, as shown in the inset of Fig. 4(a) for sample J, the dip is only observed at oblique incidence. These two features unambiguously show that the observed dip is due to L^+. In fact, theoretical calculation yields transmission minima in very good agreement with the dips observed in the heavily doped n-$In_{0.53}Ga_{0.47}As$ samples. This is shown in Fig. 4(b) for samples H and J. As can be seen in Fig. 4(b), calculations reproduce well both the frequency and the overall shape of

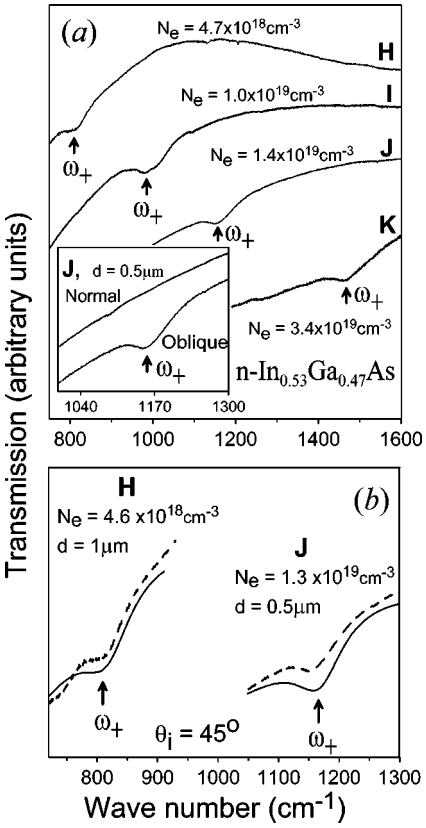

FIG. 4. (a) Infrared transmission spectra at oblique incidence of heavily doped n-$In_{0.53}Ga_{0.47}As$ samples: H, 4.7×10^{18} cm^{-3}; I, 1.0×10^{19} cm^{-3}; J, 1.4×10^{19} cm^{-3}; K, 3.4×10^{19} cm^{-3}. Inset shows a comparison between the infrared transmission of sample J obtained at normal and oblique incidence. (b) Infrared transmission calculation (solid lines) carried out for oblique incidence ($\theta_i=45°$) compared with the experimental spectra (dotted lines) of samples H and J, respectively.

the L^+ transmission dip in samples where the electron concentration differs by nearly one order of magnitude.

Given the low value of the electron effective mass in $In_{0.53}Ga_{0.47}As$, the L^+ mode exhibits large frequency shifts when the electron concentration is changed. This makes the optical determination of the electron density from the L^+ mode frequency a particularly sensitive technique for this material. The N_e and Γ_e values obtained from the fits are displayed in Table II. Although an overall good agreement is found between the electrical measurements and the results of the L^+ fits over the entire electron concentration range, we note that the electron density values obtained from the IR measurements are systematically below those obtained from the Raman and the electrical measuremenets. The reason for these discrepancies may be the uncertainity in determining the precise location of the L^+ transmission dip, which is usually observed on top of a strong and steep transmission background. Furthermore, we note that the L^+ dip is slightly asymmetric and exhibits a tail towards high frequencies, which may explain the systematic underestimate of the electron density obtained from the IR measurements. This is in contrast with the well defined and highly symmetrical L^+ peaks observed in Raman epxeriments[10] which allow line shape fits to be made accurately. However, noting that electrical determinations of the electron density, particularly by CV, are also affected by a certain degree of uncertainity, the Berreman technique provides consistent N_e values over the entire concentration range, making it a feasible alternative optical method for the determination of free-carrier density in doped semiconductor layers.

As in the case of the n-GaAs samples studied in the previous section, no L^- signature was observed in n-InGaAs samples. The reasons for the absence of L^- in n-GaAs are equally valid for n-InGaAs. In addition, the L_0 mode has also

TABLE II. List of the $In_{0.53}Ga_{0.47}As$ layers studied in this work. d is the nominal thickness of the epilayers. The third column lists the observed ω_+ frequencies. The free-electron density values N_e listed in the fourth column were determined by Hall effect and CV measurements for the $In_{0.53}Ga_{0.47}As$ samples. The fifth and sixth columns list, respectively, the free-electron concentration and damping parameters obtained from fitting the theoretical curves to the experimental transmission spectra at oblique incidence.

Sample	d (μm)	ω_+ (cm^{-1})	N_e (cm^{-3})	N_e^{IR} (cm^{-3})	Γ_e^{IR} (cm^{-1})	N_e^{Raman} (cm^{-3})[a]	Γ_e^{Raman} (cm^{-1})[a]
E	1		undoped				
F	1	278	1.1×10^{17} [b]	8.2×10^{16}	10	1.3×10^{17}	25
G	1	285	1.8×10^{17} [b]	1.6×10^{17}	20	1.8×10^{17}	20
H	1	805	4.7×10^{18} [b]	4.6×10^{18}	75	5.4×10^{18}	36
I	0.5	981	1.0×10^{19} [c]	7.9×10^{18}	100	9.0×10^{18}	43
J	0.5	1151	1.4×10^{19} [c]	1.3×10^{19}	110	1.5×10^{19}	52
K	0.5	1465	3.4×10^{19} [c]	2.7×10^{19}	125	3.2×10^{19}	69

[a]Reference 10.
[b]CV measurements.
[c]Hall measurements.

not been observed. For small N_e, even though this mode starts out as InAs-like LO, hence sharp, it is weak due to low N_e. For large N_e, it is too close to the GaAs-like TO, thus dominated by it. For the intermediate values of N_e, L_0 is plasmon-like in character and broad; the close proximity of InAs-like and GaAs-like TO's further prevents its observation.

VI. CONCLUSIONS

The results on the transmission Berreman experiments demonstrate that signatures associated with the L^+ coupled plasmon mode in doped epilayers can be successfully observed. Transmission dips are observed at oblique incidence that are not present in the spectra acquired at normal incidence, which demonstrates the longitudinal character of the excited modes.

The difficulty of observing the L^- mode in the Berreman transmission experiments appear to be due to the large plasmon-like line width as well as a decrease in strength for small N_e, on the one hand, and the close proximity of the strong and broad TO signature at high N_e on the other hand. In the particular case of $In_{0.53}Ga_{0.47}As$, the close proximity of the wide TO modes of the two sublattices also prevents the observation of the weak L_0 mode.

The L^+ mode exhibits large higher-frequency shifts with increasing electron concentration, and its frequency can be accurately measured in the infrared transmission experiments at oblique incidence. This permits the use of infrared transmission as a sensitive optical technique to determine the free-carrier density in doped semiconductor layers by fitting theoretical transmission curves. The technique has been demonstrated with *n* GaAs as well as the ternary $In_{0.53}Ga_{0.47}As$ alloy, and the carrier concentrations obtained from the fits to the transmission spectra show good agreement with electrical and Raman measurements. For $In_{0.53}Ga_{0.47}As$, the L^+ coupled mode frequency is particularly sensitive to free-charge density due to the small electron effective mass, endowing a high sensitivity to this technique.

ACKNOWLEDGMENTS

This work was partially supported by the Spanish Ministry of Science and Technology. J.I. acknowledges financial support from the Spanish Ministry of Education and Culture and S.H. from the Departament d'Universitats i Recerca de la Generalitat de Catalunya. The work carried out at Purdue University received support from the US National Science Foundation (DMR-0102699).

*Present address: School of Physics and Astronomy, University of Nottingham, United Kingdom.

[1] W.G. Spitzer and H.Y. Fan, Phys. Rev. **106**, 882 (1957).
[2] I. Yokota, J. Phys. Soc. Jpn. **16**, 2075 (1961).
[3] B.B. Varga, Phys. Rev. **137**, A1896 (1965).
[4] K.S. Singwi and M.P. Tosi, Phys. Rev. **147**, 658 (1966).
[5] A. Mooradian and G.B. Wright, Phys. Rev. Lett. **16**, 999 (1966).
[6] A. Mooradian and A.L. McWhorter, Phys. Rev. Lett. **19**, 849 (1967).
[7] M.V. Klein, in *Electronic Raman Scattering* in *Light Scattering in Solids I*, edited by M. Cardona (Springer-Verlag, Heidelberg, 1983), pp. 147–204.
[8] G. Abstreiter, M. Cardona, and A. Pinczuk, *Light Scattering by Free Carrier Excitations in Semiconductors* in *Light Scattering in Solids IV*, edited by M. Cardona and G. Güntherodt (Springer-Verlag, Berlin, 1984), pp. 5–150.
[9] T. Yuasa, S. Naritsuka, M. Mannoh, K. Shinozaki, K. Yamanaka, Y. Nomura, M. Mihara, and M. Ishii, Phys. Rev. B **33**, 1222 (1986).
[10] R. Cuscó, L. Artús, S. Hernández, J. Ibáñez, and M. Hopkinson, Phys. Rev. B **65**, 35 210 (2002).
[11] H.R. Chandrasekhar and A.K. Ramdas, Phys. Rev. B **21**, 1511 (1980).
[12] R.T. Holm, J.W. Gibson, and E.D. Palik, J. Appl. Phys. **48**, 212 (1977).
[13] O.K. Kim and W.G. Spitzer, Phys. Rev. B **20**, 3258 (1979).
[14] D.W. Berreman, Phys. Rev. **130**, 2193 (1963).
[15] M.D. Sciacca, A.J. Mayur, E. Oh, A.K. Ramdas, S. Rodriguez, J.K. Furdyna, M.R. Melloch, C.P. Beetz, and W.S. Yoo, Phys. Rev. B **51**, 7744 (1995).
[16] P. Grosse, B. Harbecke, B. Heinz, W. Jantz, and M. Maier, Appl. Phys. A: Mater. Sci. Process. **A50**, 7 (1990). See also B. Harbecke, B. Heinz, V. Offermann, and W. Theiss, in *Optical Characterization of Epitaxial Semiconductor Layers* (Springer-Verlag, Heidelberg, 1996), Chap. 5.
[17] F. Proix and M. Balkanski, Phys. Status Solidi **32**, 119 (1969).
[18] K.L. Kliewer and R. Fuchs, Phys. Rev. **144**, 495 (1966); **150**, 573 (1966).
[19] J. Groenen, R. Carles, G. Landa, C. Guerret-Piécourt, C. Fontaine, and M. Gendry, Phys. Rev. B **58**, 10 452 (1998).
[20] N.A. Semikolenova, I.M. Nesmelova, and E.N. Khabarov, Sov. Phys. Semicond. **12**, 1139 (1978).
[21] M. Cardona, Phys. Rev. **121**, 752 (1961).
[22] U. Rösssler, Solid State Commun. **49**, 943 (1984).
[23] *Numerical Data and Functional Relationships in Science and Technology*, edited by O. Madelung, M. Schulz, and H. Weiss, Landolt-Börnstein, Vol. 17a (Springer-Verlag, Heidelberg, 1982). See also C.K. Sarkar, R.J. Nicholas, J.C. Portal, M. Razeghi, J. Chevrier, and J. Massies, J. Phys. C **18**, 2667 (1985).
[24] The values of A_2, A_4, and A_6 in $E(k)=A_2k^2+A_4k^4+A_6k^6$ are for GaAs: $A_2=5.687\times10^4$ meV Å^2, $A_4=-2.395\times10^6$ meV Å^4, $A_6=1.151\times10^8$ meV Å^6, for InGaAs: $A_2=8.383\times10^4$ meV Å^2, $A_4=-4.380\times10^6$ meV Å^4, $A_6=1.129\times10^8$ meV Å^6.
[25] M. Giehler and E. Jahne, Phys. Status Solidi B **73**, 503 (1976).
[26] See, for example, A.K. Ramdas and S. Rodriguez, Rep. Prog. Phys. **44**, 1297 (1981).
[27] T.P. Pearsall, R. Carles, and J.C. Portal, Appl. Phys. Lett. **42**, 436 (1983).